HHS Public Access

Author manuscript

J Pathol. Author manuscript; available in PMC 2017 February 01.

Published in final edited form as:

J Pathol. 2016 February ; 238(3): 446–456. doi:10.1002/path.4669.

Molecular Response of Chorioretinal Endothelial Cells to Complement Injury: Implications for Macular Degeneration

Shemin Zeng[*], **S. Scott Whitmore**[*], **Elliott H. Sohn**, **Megan J. Riker**, **Luke A. Wiley**, **Todd E. Scheetz**, **Edwin M. Stone**, **Budd A. Tucker**, and **Robert F. Mullins**

The Stephen A. Wynn Institute for Vision Research and the Department of Ophthalmology and Visual Sciences, The University of Iowa, Iowa City, Iowa, USA

Abstract

Age-related macular degeneration (AMD) is a common, blinding disease of the elderly in which macular photoreceptor cells, retinal pigment epithelium, and choriocapillaris endothelial cells ultimately degenerate. Recent studies have found that degeneration of the choriocapillaris occurs early in this disease and that this endothelial cell dropout is concomitant with increased deposition of the complement membrane attack complex (MAC) at the choroidal endothelium. However, the impact of MAC injury to choroidal endothelial cells is poorly understood. To model this event *in vitro*, and to study the downstream consequences of MAC injury, endothelial cells were exposed to complement from human serum, compared to heat inactivated serum which lacks complement components. Cells exposed to complement components in human serum showed increased labeling with antibodies directed against the MAC, time and dose dependent cell death as assessed by lactate dehydrogenase assay, and increased permeability. RNA-Seq analysis following complement injury revealed increased expression of genes associated with angiogenesis including matrix metalloproteases (MMPs) 3 and 9, and VEGF-A. The MAC-induced increase in *MMP9* RNA expression was validated using C5 depleted serum compared to C5 reconstituted serum. Increased levels of MMP9 were also determined using Western blot and zymography. These data suggest that, in addition to cell lysis, complement attack on choroidal endothelial cells promotes an angiogenic phenotype in surviving cells.

Keywords

age-related macular degeneration; complement system; endothelial cells; matrix metalloproteinases

Send correspondence to: Robert F. Mullins, PhD, Stephen A. Wynn Institute for Vision Research, 375 Newton Road, Iowa City, IA 52242, Telephone: 319-335-8222. Robert-Mullins@uiowa.edu.

*These authors contributed equally to this work.

SZ, SSW, LAW, and MJR, and TES performed experiments and/or interpreted the data analysis; SZ, SSW, EHS, EMS, LAW, TES, BAT and RFM designed and interpreted experiments and/or wrote the manuscript.

The authors have no conflicts of interest to disclose.

This is original work that has not been submitted for publication elsewhere.

RNA-Seq data are appended as Supplemental Table 1.

All RNA-Seq raw data will be made available to the public on acceptance of the manuscript.

INTRODUCTION

Age-related macular degeneration (AMD) is a complex, debilitating disorder that affects central vision. The prevalence of advanced AMD is estimated to be almost 1 in 8 in the elderly population (> 80 years of age) [1], with major differences in prevalence between different populations [1–3]. The damage to the macula in advanced AMD occurs through either atrophic changes of the retinal pigment epithelium (RPE), underlying choriocapillaris, and/or retina; or angiogenic responses of choriocapillaris endothelial cells (ECs) with migration into the RPE and/or neural retina. The events leading to the activation of the neovascular form of the disease are poorly understood.

Current insights into the pathogenesis of AMD include roles for EC dropout and aberrant complement system regulation. Loss of choriocapillaris ECs in early AMD is correlated with the presence and density of drusen, extracellular deposits that form between the RPE and choriocapillaris [4]. Drusen tend to form over the extracellular matrix domains between capillary lobules [5] and in areas of low vascular density [4]. Perfusion decreases in association with extent of drusen [6] and choroidal thinning has been described in AMD [7,8], most notably, advanced atrophic AMD[9]. In addition, whole mount studies of eyes with advanced AMD have shown that death of choriocapillaris ECs occurs at the leading edges of neovascular membranes [10]. This unexpected relationship between dropout of the normal endothelium and abnormal growth of adjacent ECs into the retina of the same eyes suggest a complex disruption of hypoxia and perfusion [11].

Aberrant complement activation is also proposed to play an important role in AMD [12,13]. Polymorphisms in genes encoding members of the complement system are strongly associated with increased risk of early and advanced AMD [12,13], particularly in the complement factor H (CFH) gene [14–17]. Human eyes genotyped for this polymorphism have increased levels of C-reactive protein [18] and the complement membrane attack complex (MAC) [19]. Interestingly, the distribution of the MAC itself is consistent with potential EC injury, showing primary localization to domains surrounding the choriocapillaris [4,17,20–22]. The abundance of the MAC increases both during normal aging and in AMD [22]. Thus, the MAC could reasonably injure choriocapillaris ECs, either lytically or sublytically.

In this report, we activated complement from human serum on the surface of the RF/6A choroidal EC line and evaluated cell injury and changes in gene expression. ECs responded to complement injury by upregulating expression of classes of genes associated with angiogenesis. These findings link MAC injury with the histologically observed spectrum of responses, ranging from cell death to angiogenesis, seen in AMD.

METHODS

Immunohistochemistry and immunoEM

Human donor eyes were selected from a research eye collection. All samples in this collection were obtained after full consent of the donors' families and in accordance with the Declaration of Helsinki. For some experiments, macular sections from 3 donors were labeled

with *Ulex europaeus* agglutinin-I (Vector Laboratories) and antibodies directed against the C5b-9 MAC (Dako), as described previously[4], and were imaged using a confocal microscope (DM 2500 SPE, Leica Microsystems).

For immunoEM, juxtamacular punches of RPE-choroid from three donors (ages 79 and 84 without known ocular disease, and age 66 with a macular neovascular membrane) were fixed in 4% paraformaldehyde in PBS, dehydrated, and embedded in LR White resin (Electron Microscopy Sciences) and cured with ultraviolet light on ice, according to the manufacturer's instructions. Thin sections were collected on formvar coated grids, and sections were blocked in a solution of 5% Bovine Serum Albumin-c (BSA, Electron Microscopy Sciences) with 3% goat serum (Sigma) and 0.1% cold water fish skin gelatin (Electron Microscopy Sciences). Sections were then rinsed, and incubated overnight with anti-MAC antibody. Sections were washed and incubated with goat anti-mouse IgG conjugated to 1nm gold, rinsed, crosslinked with 2% glutaraldehyde, and washed again prior to silver enhancement (Electron Microscopy Sciences) according to the manufacturer's instructions.

Cell cultures and injury model

Human serum, complement C5 from human serum and complement C5-deficient human serum used in this experiment were purchased from Sigma-Aldrich (St. Louis, MO). To inactivate complement, serum was heated in a water bath at 56°C for 1 hour. For some experiments, complement was inactivated using cobra venom factor (CVF; Quidel) at a concentration of 80 units of CVF per 1 ml of 50% human serum, and the solution was incubated for 30 minutes at 37°C before being added to the cells. In addition, for some experiments C5-deficient serum (which is unable to form the MAC) or C5-deficient serum reconstituted with 75μg/mL C5 was used as a source of complement.

The chorioretinal EC line (RF/6A) was purchased from the American Type Culture Collection (ATCC) and cultured in Dulbecco's modification of Eagle media (DMEM, Invitrogen) supplemented with 10% fetal bovine serum (FBS) and 1% penicillin-streptomycin (PS, Life Technologies). After cells reached 80%-90% confluency in T75 cm^2 flasks, cells were trypsinized and seeded into 12-well clusters (Corning) at a density of 1×10^5 cells per well in a volume of 1 mL and grown in 10% FBS DMEM and 1% PS at 37°C for 40–48 hours. The cells were washed with FBS-free DMEM twice.

To study the effects of complement activation on ECs, cells were then treated with different concentrations of human serum ranging from 5% to 100% at 37°C for 2, 4, and 24 hours. Cells were exposed to either normal serum (complement-intact) or heat inactivated serum ("HIS", complement-deficient). All steps were performed at 37°C with 5% CO_2 and 90% humidity.

Immunocytochemistry

In order to verify that the MAC was activated on the surface of ECs exposed to normal serum, HIS, C5-deficient serum, or C5 reconstituted serum, additional cells from each experiment were grown on glass coverslips or chamber slides and exposed to identical conditions as the cells used for biochemical studies. Following incubation, cells were then

fixed in 4% paraformaldehyde and labeled with antibodies directed against human MAC (Dako antibody AE9), visualized with Alexa-488 conjugated anti-mouse secondary antibodies (Invitrogen).

Quantification of cell lysis

In order to determine the susceptibility of choroidal endothelial cells to lysis after activation of complement, we performed a cell viability assay following treatment with either serum-free media, normal human serum, HIS, C5-deficient serum, or C5-deficient serum reconstituted with C5, by quantifying lactate dehydrogenase (LDH) released into the medium by lysed RF/6A cells as described previously [23]. Triton X-100 was used as a positive control to determine the abundance of LDH released following 100% lysis. LDH release was quantified using the cytotoxicity detection kit (Roche Diagnostics Corp., Indianapolis, IN) and expressed as relative cell death, compared to Triton X-100. Experiments were performed in triplicate.

Quantification of permeability

Horseradish peroxidase (HRP; Sigma-Aldrich, St. Louis, MO) was used to measure the permeability of RF/6A monolayers after complement treatment. The procedure was performed as previously described by Chen et al. [24]. RF/6A cells (5×10^5) in 200μL of 5% FBS DMEM medium with 1% penicillin/streptomycin (Life Technologies Corporation) were plated on a Transwell tissue culture insert with 0.4 μm pores (Corning, New York, NY) and the lower chamber was filled with 800μL medium. The monolayers were allowed to reach confluency and were then treated with (a) different concentrations of human serum (5%–100%); (b) 5% HIS; or (c) serum-free DMEM. Each group was evaluated in triplicate. After treatment, HRP (50 μg/mL) was added to the upper chambers. After 30 min, 5 μL were withdrawn from each well were assayed for HRP activity as described previously [24]. To quantify cell permeability, an HRP standard curve was first prepared using serial dilutions of HRP. Cell permeability was calculated as Flux (mL/cm^2) as described previously. Experiments were performed in triplicate.

Evaluation of gene expression changes

Following 4 hours of acute complement injury (serum concentration 50%), gene expression changes were evaluated using RNA-Sequencing [25]. Endothelial cells injured with MAC (n=3 wells/comparison) were compared to cells exposed to HIS (n=3). The presence of activated MAC was observed on cells exposed to serum, but not control cells, as described above. Total RNA was isolated using the RNeasy kit (Qiagen, Valencia, CA).

RNA quality control and sequencing were performed at the Genomics Division of the Iowa Institute of Human Genetics at The University of Iowa. RNA quality was determined on a Bioanalyzer (Agilent Technologies, Santa Clara, CA) and samples with an RNA Integrity Number of greater than 9 were employed. Briefly, the TruSeq RNA Sample Preparation v2 Library preparation kit (Illumina, Cat. #15026495) was employed to generate libraries for sequencing on the HiSeq 2000 platform according to the manufacturer's instructions. Three hundred nanograms of total RNA were fragmented, converted to cDNA and ligated to

sequencing adaptors containing barcodes. Libraries were validated and normalized, and pooled samples were then sequenced using a 2 × 100 nt paired-end run on a HiSeq 2000.

Bioinformatics

Read alignment was performed using Tophat (ver. 2.0.7) to *Macaca mulatta* genome build Mmul_1 (Illumina iGenomes; http://support.illumina.com/sequencing/sequencing_software/igenome.ilmn). Tophat2 was run with inner mate pair distance (-r) set to 150, no coverage search specified, and library type set to "fr-unstranded". Transcript definitions (i.e., GTF) used were those provided in the iGenomes bundle. Junction mapping and transcript abundance was calculated using Cufflinks (ver. 2.1.1) [26] with max-bundle-frags set to 20,000,000. Differential expression was calculated using Cuffdiff (ver. 2.1.1) and CummeRbund (ver. 2.2.0) with GTF set to that provided in the iGenomes package. Isoforms were considered to be significantly differentially expressed if the fold change was ≥ 2 and the q-value ≤ 0.001. Enrichment with human Gene Ontology (GO) terms was determined using WebGestalt (http://bioinfo.vanderbilt.edu/webgestalt/). Gene identifiers were treated as human gene symbols, and all genes in the human genome were used as background for statistical calculations. P-values were calculated using a hypergeometric probability density function for GO terms with at least five genes. Terms were considered significantly enriched if the Bonferrroni corrected $p<0.01$.

We verified the rhesus macaque origin of our cells by genotyping our RNA-Seq reads. Briefly, we used Clustal Omega algorithm (http://www.ebi.ac.uk/Tools/msa/clustalo/) to align the mRNA sequences of *ICAM1* from rhesus (NM_001047135.1) and human (NM_000201.2). Within the 1605bp region of overlap between the two sequences, we selected a common 18bp region (CCGTTGCCTAAAAAGGAG) shared by both organisms that was bordered on either side by sequence differences. Using this sequence, we queried one of the control samples (FASTQ file) with the common sequence to identify 123 overlapping reads. We then aligned these RNA-Seq reads, the 18 bp query, NM_001047135.1, and NM_000201.2 using Clustal Omega. From the aligned reads, we recovered a 175bp region encompassing 23 differences between rhesus and human sequence.

Validation of increased expression

Expression of *MMP9* was evaluated by quantitative PCR using the ddCT method as described previously [23]. Primer sequences of MMP9 and its reference gene, *RPL19*, were selected as follows: *MMP9*, Forward, 5′-CGAGAGACTCTACACCCAGGA-3′ and Reverse, 5′-AGGAAGGTGAAGGGGAAAAC-3′, and RPL19, Forward, 5′-ATGCCAACTCCCGTCAGC-3′and Reverse, 5′-ACCCTTCCGCTTACCTATGC-3′.

In addition, ELISA analysis was performed for VEGFA using a commercial kit (RayBiotech) according to the manufacturer's instructions on supernatants of cells exposed to 20% human serum, 20% HIS, 20% C5-deficient serum, and 20% C5-deficient serum reconstituted with C5, as above.

Western blot analysis was performed for MMP9 as described previously [23]. RF/6A cells were treated with (a) 20–50% human serum; (b) 20–50% HIS; and (c) serum-free DMEM. After injury, cells were washed twice with DMEM medium and incubated with serum-free

DMEM with 1% penicillin-streptomycin for 12 hours. The conditioned medium was collected, centrifuged at 406×g for 5 minutes to remove detached cells, and concentrated with 30kDa cutoff spin columns (Millipore). Proteins were separated using SDS-PAGE and transferred onto a polyvinylidene difluoride membrane (Millipore). Antibodies directed against MMP9 (ab13458, Millipore, Billerica, MA) were diluted to 10 μg/mL and were detected with HRP-conjugated secondary antibodies (GE Healthcare) using a chemiluminescence kit (Bio-Rad).

Zymography

Gelatin zymography was performed using precast gelatin zymography gels (Bio-Rad, Hercules, CA). For each sample, 35 μg concentrated supernatant protein was diluted in zymography loading buffer (Bio-Rad, Hercules, CA) and loaded into each lane. Following electrophoretic separation, MMPs were activated with Zymogram Renaturing Buffer (Bio-Rad, Hercules, CA) and stained with Coomassie blue R-250.

RESULTS

High resolution microscopy/ImmunoEM

Frozen sections of 3 donors were evaluated by confocal microscopy. Confocal microscopy shows anti-MAC reactive material surrounding the choriocapillaris, as has been described previously, with the majority of the signal in the perivascular domain (Figure 1A). These profiles appear punctate in confocal optical sections, especially on the vitread, fenestrated surface of the endothelium. At higher magnifications, there is evidence of MAC accumulation internal to the choriocapillaris basal lamina and overlapping the endothelium (visualized by UEA-I lectin, Figure 1B).

LR White embedded sections were evaluated using immunoEM for the MAC. Labeling was strongest in Bruch's membrane, with rare but notable labeling observed on the surface of choriocapillaris ECs (Figure 1C). Positive labeling was compared to secondary antibody alone (Figure 1D), which showed rare scattered particles. While several labeling events on the choriocapillaris were observed in the presence of anti-MAC antibody, this was not observed with secondary antibody alone--in over 100 control fields evaluated, labeling was not observed on the endothelium

Complement activation

RF/6A cells exposed to normal human serum or C5-depleted serum reconstituted with C5, exhibited robust cell surface labeling with antibodies directed against MAC, whereas cells incubated with HIS or with C5-depleted serum did not display surface labeling with anti-MAC antibodies (Figure 2A–D).

Cytolysis assays

The LDH cytotoxicity assay was used to quantify cell death following exposure to the MAC. We employed 2 dilutions of normal human serum (5% and 10%) to treat cultured RF/6A cells and measured LDH release after 4–48 hours. The estimated relative cell death (RCD, the measured LDH activity divided by the LDH activity following 100% cell lysis of

identical wells with Triton X-100) was significantly increased after 4 hours in both 5% and 10% normal serum compared to HIS ($p<0.05$) (Figure 3A). Relative cell death was significantly elevated at all subsequent time points (Figure 3A). To determine the impact of C5 depletion on cytolysis in this system, we also investigated the cytotoxicity of C5-sufficient and C5-deficient human serum on cultured RF/6A cells. C5-deficient serum (20%) reconstituted with C5 showed a significantly higher level of cell death than C5-deficient serum alone ($p<0.01$) (Figure 3B), although reconstituted serum was slightly less effective at killing cells than normal human serum. Both HIS and C5-depleted serum showed increased cell death compared to medium alone (Figure 3), suggesting mild toxicity due to non-complement activities in serum.

Endothelial cell permeability

To determine the role of complement injury on EC permeability, we used a series of concentrations of human serum to treat RF/6A cells and measured the cell monolayer permeability to horseradish peroxidase (HRP). After 24 hours of treatment, permeability was significantly increased in all concentrations compared to the 5% HIS group (all $p<0.05$). There was no statistical difference between the 5% HIS group and the serum free group ($p>0.05$) (Figure 4).

Cell line validation

The *Macaca mulatta* provenance of the RF/6A cells used in these experiments was validated using RNA-Seq. Comparison of species-specific variants in the *ICAM1* gene was performed. A 175 bp region encompassing 23 differences between rhesus and human sequence was evaluated. At these 23 sites, the overwhelming majority of aligned bases matched the rhesus nucleotide, with the departures from the *Macaca* sequence likely due to rare sequencing errors (Supplemental Figure 1).

Gene expression

Gene expression was evaluated following MAC injury in RF/6A cells. A minimum of 20 million paired end reads were obtained per sample (21,676,942 to 29,135,734). A total of 15,108 transcripts were considered reliably expressed (minimum FPKM value for all samples in either group greater than or equal to 1). Of these genes, 541 transcripts increased expression upon MAC treatment (fold change ≥ 2 and q-value less than or equal to 0.001), whereas 602 transcripts decreased expression upon MAC treatment (fold change ≤ -2 and q-value ≤ 0.001; Table 1). Raw data from this experiment will be submitted to Gene Expression Omnibus and processed data are uploaded as Supplemental Table 1. Interestingly, of the top 20 increased transcripts, at least 12 are associated with angiogenesis or vasculogenesis.

For pathway analysis, we limited our investigation of gene enrichment in differentially expressed genes to gene ontology (GO) terms designated as part of a “biological process”. Within the top 200 genes with most increased expression upon complement treatment, WebGestalt identified 40 GO terms that were significantly enriched (Bonferroni corrected $p<0.01$). No GO terms were enriched in the 200 genes with most decreased expression upon MAC treatment. WebGestalt represents enriched GO terms as a directed acyclic graph, a

hierarchical structure derived from the underlying ontology, with more general terms (e.g, “multicellular organismal development”) appearing higher in the structure than more specific terms (e.g., “circulatory system development”). To further refine the GO analysis, we focused on terms in the graph lacking “child” terms, listed in Table 2. Thus, the most specific, enriched term contains twenty-four genes involved in blood vessel morphogenesis, including *VEGFA*.

Confirmation of gene expression changes

Quantitative PCR was performed on additional wells of cells treated with complement or a series of controls. Increased *MMP9* expression at the RNA level was confirmed at 4 hours following 50% serum exposure (>9× fold change compared to HIS, $p<0.05$, normalized to *RPL19*; Supplemental Figure 2).

In order to rule out the possibility that expression changes in *MMP9* were due to other undefined components of serum that may have been denatured by the heat inactivation step, cells were treated with either C5-deficient serum or C5-deficient serum reconstituted with C5, and *MMP9* mRNA levels were determined using quantitative RT-PCR. Compared to C5-deficient serum, adding C5 significantly increased *MMP9* expression after 4 hours (>2 fold increase, $p<0.01$), with levels returning to baseline after 24 hours ($p>0.05$). Similarly, cells exposed to CVF-treated serum did not differ in *MMP9* expression from cells exposed to HIS ($p>0.05$), but showed significantly lower MMP9 than 50% normal serum-treated cells (>3 fold decrease, $p<0.05$; Supplemental Figure 2).

ELISA analysis of VEGF-A revealed a small but significant increased VEGF-A protein in 20% serum treated—compared to 20% HIS-treated—cell conditioned media after 8 hours ($p<0.05$); Supplemental Figure 3. Western blots of the conditioned media of 50% normal serum exposed RF/6A cells with an antibody directed against MMP9 showed an increased abundance of a series of immunoreactive bands (ranging from 40 to 150 kDa), compared to HIS exposed cells or cells exposed to serum free medium (Figure 5A).

To assess whether the increased MMP9 in complement treated cells is functional, zymography analysis was performed. Cells exposed to 50% normal serum exhibited remarkably higher gelatinase activity at 88kDa (a profile unique to the complement treated cells; Figure 5B). Serum alone did not possess this activity.

DISCUSSION

In this report, we describe the effects of complement exposure on choroidal ECs in a system that models some aspects of AMD. Our results indicate that the choriocapillaris is exposed to the MAC and that choroidal ECs are susceptible to complement-mediated cytolysis in a concentration- and dose-dependent manner. As discussed above, several lines of evidence suggest that injury of choriocapillaris ECs by MAC deposition is a major driving pathological insult leading to AMD (reviewed in [27]). In contrast, except in some cases of choroidal neovascularization (CNV) [22], robust MAC deposition on the RPE is not observed. This observation may be due to differential protection of RPE and ECs: while the RPE expresses high levels of CD46, a negative complement regulator, the choriocapillaris

may be less equipped to shield itself from MAC [28,29], possibly relying more on CFH for protection. Given the high level of exposure of choroidal ECs to MAC in even young eyes [22], any impairment of complement inhibition could lead to damage to ECs. Once the loss of capillary ECs overcomes the rate of replacement, decreased perfusion is a likely consequence.

We recently described an increase in the density of “ghost” vessels (remnants of viable capillaries that are no longer occupied by endothelial cells) with increasing drusen density [4]. Thus, the MAC has the means to harm ECs (as described in the current study), shows increased activation in AMD-associated CFH polymorphisms [19], and has been frequently observed in close proximity with the cells lost first in early AMD (the choriocapillaris endothelium) [17,21,22]. For these reasons, compelling circumstantial evidence supports a role for MAC in the damage observed in the choriocapillaris. Interestingly, this observation is specific to choriocapillaris as capillary beds in other tissues do not show a similar age-related MAC accumulation [30].

In addition to cell death, the activation of the complement system can also change the phenotype of cells exposed to its components. We [21] and others [31] have studied the impact of complement anaphylatoxins on choriocapillaris and/or RPE cells. In order to better understand the impact of MAC injury, in the current report we sought to characterize the changes in cell phenotype using gene expression analysis. Our RNA-Seq analysis indicates that acute MAC injury of choroidal ECs leads to rapidly increased expression of genes involved in blood vessel formation, a set of genes likely upregulated in CNV formation.

The upregulation of MMP9 expression is especially interesting in light of a compelling body of work on RPE cells injured by MAC [32]. Induction of MMP9 expression by complement-injured choriocapillaris could lead to localized degradation of the choriocapillaris basal lamina, a critical first step in angiogenesis [33]. It is also notable that serum with C5 induced elevated MMP9 expression, indicating that this increase is not solely due to C3 activation.

A scenario with the paradoxical features of both EC death and increased angiogenesis (in surviving cells) following complement attack would comport well with observations made on human eyes by McLeod and coworkers, in which capillary dropout, with preserved RPE, was found adjacent to choroidal neovascular membranes[10]. In our proposed model, MAC-induced EC dropout may occur either before or concurrently with the induction of angiogenesis. Induction of pro-angiogenic genes could then trigger rapid, uncontrolled growth of blood vessels, leading to the formation of a neovascular membrane. In other words, MAC-exposed choroidal ECs may alternatively be damaged beyond repair or be sublytically injured, resulting in activation of a gene expression program that promotes angiogenesis.

The mechanistic link between complement activation and CNV has been advanced since at least 2005, when Bora et al. determined that systemic complement inhibition with CVF or by C3 deficiency impaired the growth of new blood vessels into a site of laser injury [34]; these findings have been further validated in mice with genetically targeted deletions in

other genes associated with the complement system and in animals treated with natural or synthetic inhibitors of complement [35–38]. The current study further suggests that MAC deposition acts directly on choroidal ECs to either lyse the cells or to promote conversion to a proangiogenic phenotype.

The current study has several limitations. Although the relevance of the study is directed toward AMD, a largely human disease, we employed a cell line form rhesus macaque (RF/6A). The advantage of these cells is that, since they are immortal, the same line of cells can be used for multiple experiments with good reproducibility. Orthologs in Macaca mulatta is >97% identical to human at the nucleotide level [39], and Macaca is one of the few (if not the only) non-human genus to develop an AMD-like phenotype [40],[41]. A second limitation relates to the injury model itself. While we demonstrate that the membrane attack complex is deposited on the surface of serum-exposed EC, it is possible that not all of the observed cellular responses are due to the deposition of MAC. Indeed, even C5-depleted serum, while showing less cytolysis than reconstituted serum, showed increased cytolysis compared to medium alone. This response may be due to the presence of anti-endothelial antibodies in human serum, which have been described previously [42] or the effects of anaphylatoxins such as C3a [43]. However, when normalized to C5-deficient serum or CVF-activated serum, the serum that forms MAC on the cell surface leads to increased MMP9 expression and increased cell loss, implicating complement directly.

Given the involvement of MAC deposition in normal aging and early AMD, we suggest that future therapeutic approaches may seek to augment the resistance of choroidal ECs against MAC injury prior to the development of atrophy or neovascularization.

Supplementary Material

Refer to Web version on PubMed Central for supplementary material.

Acknowledgments

Supported in part by: NIH grants EY-024605, EY-023187, and 1-DP2-OD007483-01; the Elmer and Sylvia Sramek Charitable Foundation; The Ronald and Annette Massman Choroideremia Research Fund; the Howard F. Ruby Endowment for Human Retinal Engineering; the Stephen A. Wynn Foundation; the Hansjoerg E.J.W. Kolder, M.D., Ph.D., Professorship in Best Disease Research; and the Martin and Ruth Carver Chair in Ocular Cell Biology.

References

1. Klein R, Klein BEK. The prevalence of age-related eye diseases and visual impairment in aging: current estimates. Invest Ophthalmol Vis Sci. 2013 Dec; 54(14):ORSF5–ORSF13. [PubMed: 24335069]
2. Buitendijk GHS, Rochtchina E, Myers C, et al. Prediction of Age-related Macular Degeneration in the General Population: The Three Continent AMD Consortium. Ophthalmology. 2013 Oct 10; 120(12):2644–55. [PubMed: 24120328]
3. Klein R, Chou C-F, Klein BEK, et al. Prevalence of age-related macular degeneration in the US population. Arch Ophthalmol. 2011 Jan; 129(1):75–80. [PubMed: 21220632]
4. Mullins RF, Johnson MN, Faidley EA, et al. Choriocapillaris vascular dropout related to density of drusen in human eyes with early age-related macular degeneration. Invest Ophthalmol Vis Sci. 2011 Mar; 52(3):1606–12. [PubMed: 21398287]

5. Lengyel I, Tufail A, Hosaini HA, et al. Association of drusen deposition with choroidal intercapillary pillars in the aging human eye. Invest Ophthalmol Vis Sci. 2004 Sep; 45(9):2886–92. [PubMed: 15326099]
6. Berenberg TL, Metelitsina TI, Madow B, et al. The association between drusen extent and foveolar choroidal blood flow in age-related macular degeneration. Retina (Philadelphia, Pa). 2012 Jan; 32(1):25–31.
7. Ko A, Cao S, Pakzad-Vaezi K, et al. Optical coherence tomography-based correlation between choroidal thickness and drusen load in dry age-related macular degeneration. Retina (Philadelphia, Pa). 2013 May; 33(5):1005–10.
8. Hu Z, Wu X, Ouyang Y, et al. Semiautomated segmentation of the choroid in spectral-domain optical coherence tomography volume scans. Invest Ophthalmol Vis Sci. 2013; 54(3):1722–9. [PubMed: 23349432]
9. Sohn EH, Khanna A, Tucker BA, et al. Structural and Biochemical Analyses of Choroidal Thickness in Human Donor Eyes. Invest Ophthalmol Vis Sci. 2014 Feb 11.
10. McLeod DS, Grebe R, Bhutto I, et al. Relationship between RPE and choriocapillaris in age-related macular degeneration. Invest Ophthalmol Vis Sci. 2009 Oct; 50(10):4982–91. [PubMed: 19357355]
11. Bhutto I, Lutty G. Understanding age-related macular degeneration (AMD): relationships between the photoreceptor/retinal pigment epithelium/Bruch's membrane/choriocapillaris complex. Mol Aspects Med. 2012 Aug; 33(4):295–317. [PubMed: 22542780]
12. Anderson DH, Radeke MJ, Gallo NB, et al. The pivotal role of the complement system in aging and age-related macular degeneration: hypothesis re-visited. Prog Retin Eye Res. 2010 Mar; 29(2): 95–112. [PubMed: 19961953]
13. Khandhadia S, Cipriani V, Yates JRW, et al. Age-related macular degeneration and the complement system. Immunobiology. 2012 Feb; 217(2):127–46. [PubMed: 21868123]
14. Haines JL, Hauser MA, Schmidt S, et al. Complement factor H variant increases the risk of age-related macular degeneration. Science. 2005 Apr 15; 308(5720):419–21. [PubMed: 15761120]
15. Klein RJ, Zeiss C, Chew EY, et al. Complement factor H polymorphism in age-related macular degeneration. Science. 2005 Apr 15; 308(5720):385–9. [PubMed: 15761122]
16. Edwards AO, Ritter R, Abel KJ, et al. Complement factor H polymorphism and age-related macular degeneration. Science. 2005 Apr 15; 308(5720):421–4. [PubMed: 15761121]
17. Hageman GS, Anderson DH, Johnson LV, et al. A common haplotype in the complement regulatory gene factor H (HF1/CFH) predisposes individuals to age-related macular degeneration. Proc Natl Acad Sci USA. 2005 May 17; 102(20):7227–32. [PubMed: 15870199]
18. Johnson PT, Betts KE, Radeke MJ, et al. Individuals homozygous for the age-related macular degeneration risk-conferring variant of complement factor H have elevated levels of CRP in the choroid. Proc Natl Acad Sci USA. 2006 Nov 14; 103(46):17456–61. [PubMed: 17079491]
19. Mullins RF, Dewald AD, Streb LM, et al. Elevated membrane attack complex in human choroid with high risk complement factor H genotypes. Exp Eye Res. 2011 Oct 1; 93(4):3–3.
20. Seth A, Cui J, To E, et al. Complement-associated deposits in the human retina. Invest Ophthalmol Vis Sci. 2008 Feb; 49(2):743–50. [PubMed: 18235023]
21. Skeie JM, Fingert JH, Russell SR, et al. Complement component C5a activates ICAM-1 expression on human choroidal endothelial cells. Invest Ophthalmol Vis Sci. 2010 Oct; 51(10):5336–42. [PubMed: 20484595]
22. Mullins RF, Schoo DP, Sohn EH, et al. The Membrane Attack Complex in Aging Human Choriocapillaris: Relationship to Macular Degeneration and Choroidal Thinning. Am J Pathol. 2014 Sep 7.
23. Zeng SS, Hernández JJ, Mullins RF. Effects of Antioxidant Components of AREDS Vitamins and Zinc Ions on Endothelial Cell Activation: Implications for Macular Degeneration. Invest Ophthalmol Vis Sci. 2012 Feb 1; 53(2):1041–7. [PubMed: 22247465]
24. Chen Y-H, Xu X, Sheng M-J, et al. Effects of asymmetric dimethylarginine on bovine retinal capillary endothelial cell proliferation, reactive oxygen species production, permeability, intercellular adhesion molecule-1, and occludin expression. Mol Vis. 2011; 17:332–40. [PubMed: 21297899]

25. Whitmore SS, Wagner AH, Deluca AP, et al. Transcriptomic analysis across nasal, temporal, and macular regions of human neural retina and RPE/choroid by RNA-Seq. Exp Eye Res. 2014 Dec. 129:93–106. [PubMed: 25446321]
26. Trapnell C, Williams BA, Pertea G, et al. Transcript assembly and quantification by RNA-Seq reveals unannotated transcripts and isoform switching during cell differentiation. Nat Biotechnol. 2010 May; 28(5):511–5. [PubMed: 20436464]
27. Whitmore SS, Sohn EH, Chirco KR, et al. Complement activation and choriocapillaris loss in early AMD: Implications for pathophysiology and therapy. Prog Retin Eye Res. 2014 Dec 5.
28. Ebrahimi KB, Fijalkowski N, Cano M, et al. Decreased membrane complement regulators in the retinal pigmented epithelium contributes to age-related macular degeneration. J Pathol. 2013 Apr; 229(5):729–42. [PubMed: 23097248]
29. Vogt SD, Barnum SR, Curcio CA, et al. Distribution of complement anaphylatoxin receptors and membrane-bound regulators in normal human retina. Exp Eye Res. 2006 Oct; 83(4):834–40. [PubMed: 16764856]
30. Chirco KR, Tucker BA, Stone EM, et al. Selective Accumulation of the Complement Membrane Attack Complex in Aging Choriocapillaris. Exp Eye Res. 2015 Sep 11.
31. Nozaki M, Raisler BJ, Sakurai E, et al. Drusen complement components C3a and C5a promote choroidal neovascularization. Proc Natl Acad Sci USA. 2006 Feb 14; 103(7):2328–33. [PubMed: 16452172]
32. Bandyopadhyay M, Rohrer B. Matrix metalloproteinase activity creates pro-angiogenic environment in primary human retinal pigment epithelial cells exposed to complement. Invest Ophthalmol Vis Sci. 2012 Apr; 53(4):1953–61. [PubMed: 22408008]
33. Sang QX. Complex role of matrix metalloproteinases in angiogenesis. Cell Res. 1998 Sep; 8(3): 171–7. [PubMed: 9791730]
34. Bora PS, Sohn J-H, Cruz JMC, et al. Role of complement and complement membrane attack complex in laser-induced choroidal neovascularization. J Immunol. 2005 Jan 1; 174(1):491–7. [PubMed: 15611275]
35. Bora NS, Kaliappan S, Jha P, et al. Complement activation via alternative pathway is critical in the development of laser-induced choroidal neovascularization: role of factor B and factor H. J Immunol. 2006 Aug 1; 177(3):1872–8. [PubMed: 16849499]
36. Rohrer B, Coughlin B, Kunchithapautham K, et al. The alternative pathway is required, but not alone sufficient, for retinal pathology in mouse laser-induced choroidal neovascularization. Mol Immunol. 2011 Mar; 48(6–7):e1–8. [PubMed: 21257205]
37. Rohrer B, Long Q, Coughlin B, et al. A targeted inhibitor of the alternative complement pathway reduces angiogenesis in a mouse model of age-related macular degeneration. Invest Ophthalmol Vis Sci. 2009 Jul; 50(7):3056–64. [PubMed: 19264882]
38. Birke K, Lipo E, Birke MT, et al. Topical application of PPADS inhibits complement activation and choroidal neovascularization in a model of age-related macular degeneration. PLoS ONE. 2013; 8(10):e76766. [PubMed: 24130789]
39. Gibbs RA, Rogers J, et al. Rhesus Macaque Genome Sequencing and Analysis Consortium. Evolutionary and biomedical insights from the rhesus macaque genome. Science. 2007 Apr 13; 316(5822):222–34. [PubMed: 17431167]
40. Gouras P, Ivert L, Landauer N, et al. Drusenoid maculopathy in rhesus monkeys (Macaca mulatta): effects of age and gender. Graefes Arch Clin Exp Ophthalmol. 2008 Oct; 246(10):1395–402. [PubMed: 18709381]
41. Iwata T. Complement activation of drusen in primate model (Macaca fascicularis) for age-related macular degeneration. Adv Exp Med Biol. 2007; 598:251–9. [PubMed: 17892217]
42. Morohoshi K, Patel N, Ohbayashi M, et al. Serum autoantibody biomarkers for age-related macular degeneration and possible regulators of neovascularization. Exp Mol Pathol. 2012 Feb; 92(1):64–73. [PubMed: 22001380]
43. Ramos de Carvalho JE, Klaassen I, Vogels IMC, et al. Complement factor C3a alters proteasome function in human RPE cells and in an animal model of age-related RPE degeneration. Invest Ophthalmol Vis Sci. 2013; 54(10):6489–501. [PubMed: 23982842]

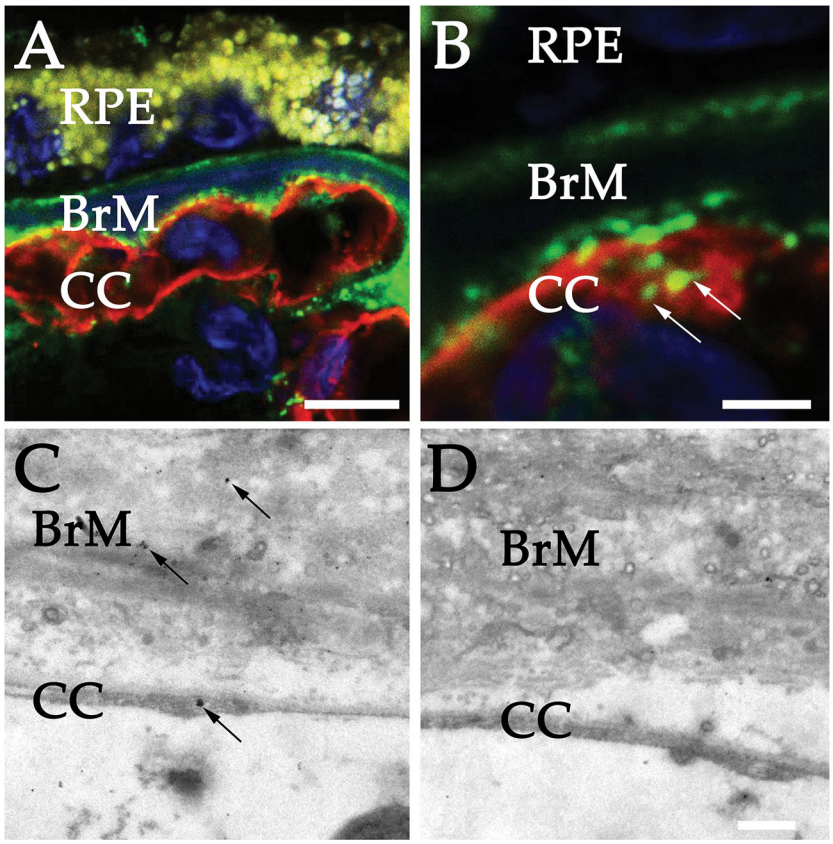

Figure 1.

High resolution detection of complement complexes in the human choriocapillaris. (A) Confocal microscopy of MAC (green) and UEA-I (red). Note the punctate MAC reactivity along the vitread surface of the choriocapillaris. Higher magnification (B) shows regional colocalization of MAC with the EC cell surface (arrows). (C) ImmunoEM localization of the membrane attack complex in human choroid. Section incubated with anti-MAC antibody shows labeling in the extracellular matrix of Bruch's membrane (BrM); in addition, labeling is observed on a choroidal EC (arrow). (D) Section from the same eye incubated with secondary antibody alone. Scale bars = 10μm (A), 2.5μm (B), 500nm (D).

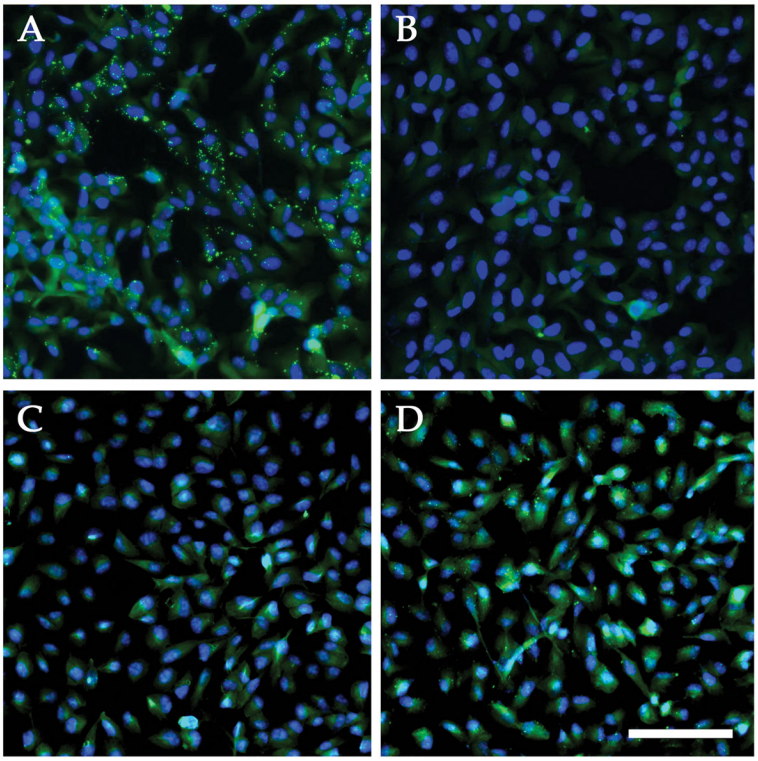

Figure 2.

Immunocytochemistry of activated membrane attack complex on primate ECs. Labeling with an anti-MAC antibody (green) was remarkable on cells exposed to 50% normal serum (A), but labeling was not observed in the presence of heat-inactivated serum (B). Cells in C5-depleted serum failed to activate complement (C), unless the serum was reconstituted with C5 (D). Exposure and level adjustments were identical between A& B and C & D, respectively. Blue counterstain, DAPI. Scalebar = 100μm.

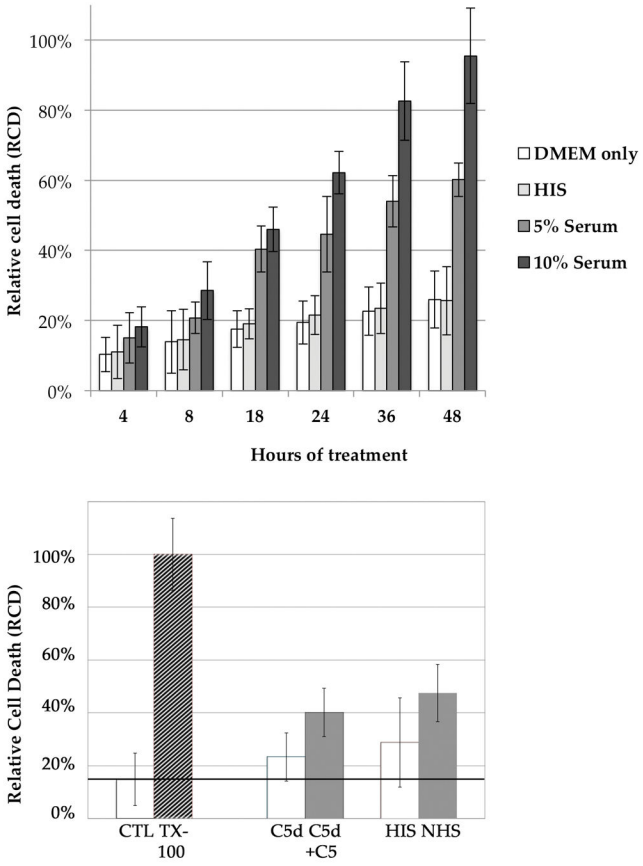

Figure 3.

Cytolysis of ECs with complement-depleted and complement-containing serum. (A) Relative cell death of normal human serum-treated (5% and 10%) and heat-inactivated serum (HIS, 5%) over the course of 24hr. Compared to HIS treated cells, a higher RCD appeared in both serum-treated groups at all time points ($p<0.05$). (B) Relative cell death after 4 hours following exposure to medium alone, medium with Triton X-100 (defined as 100% cell death), 20% C5-deficient serum, 20% C5-deficient serum reconstituted with C5, 20% heat inactivated serum (HIS), and 20% normal human serum (NHS). RCD was significantly higher in cells exposed to complement. Horizontal line shows level of cell death estimated in medium-alone exposed cells. Error bars indicate standard deviation. * $p<0.01$.

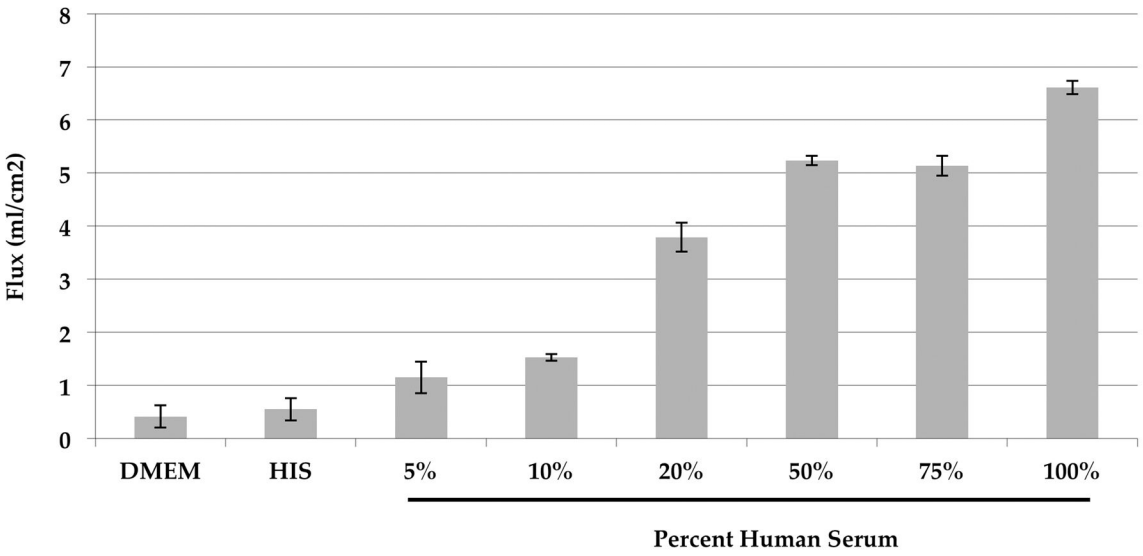

Figure 4.

EC permeability after exposure to complement-intact serum compared to complement-inactivated serum. A dose- and time-dependent increase in transendothelial flux (mL/cm^2) was observed in RF/6A cells following complement injury. An increased flux occurred in 5% to 100% normal serum-treated cells compared to 5% HIS and serum-free medium after 24 hours of treatment ($p<0.05$).

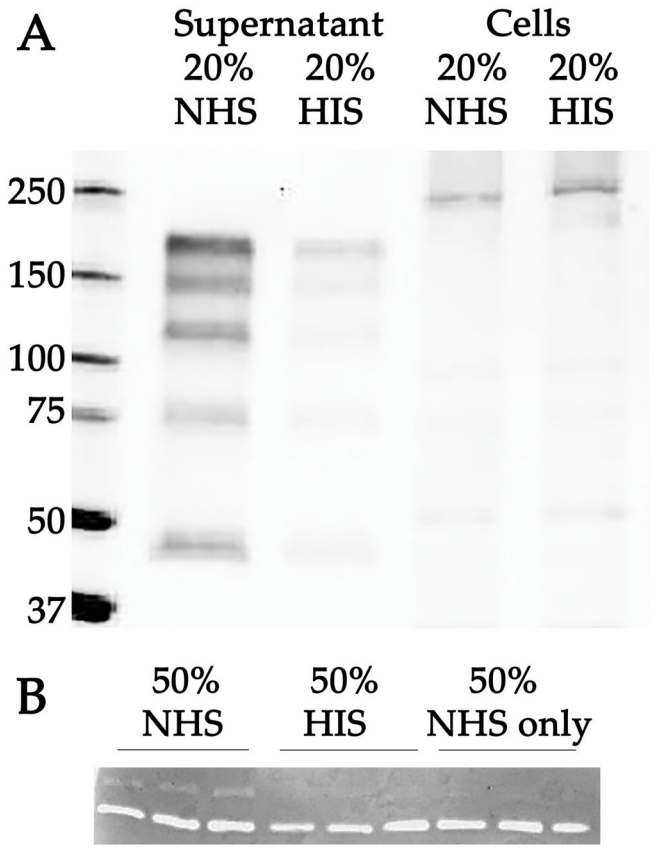

Figure 5.

Western blot of MMP9 (A) and zymography (B) following exposure of RF/6A cells to complement. Blot (A) shows reactivity of anti-MMP9 antibody to conditioned media of cells treated with 20% normal serum (NHS); conditioned media of cells treated with 20% heat inactivated serum (HIS); and extracts of cells following exposure to NHS and HIS, respectively. After 4 hours, a series of immunoreactive bands was significantly elevated in the conditioned medium of treated cells compared to controls exposed to complement depleted serum. (B) Zymography analysis of MMP activity using conditioned media from cells exposed to 50% normal serum or 50% HIS, or from medium alone that was not conditioned by EC ("50% NHS only"). Three individual samples are depicted for each group. All samples showed a band of gelatinase activity at approximately 65. An 88 kDa gelatin-cleaving band was observed only in the normal serum-treated cells, compared to both HIS conditioned medium and serum containing non-conditioned media control groups, after 4 hours.

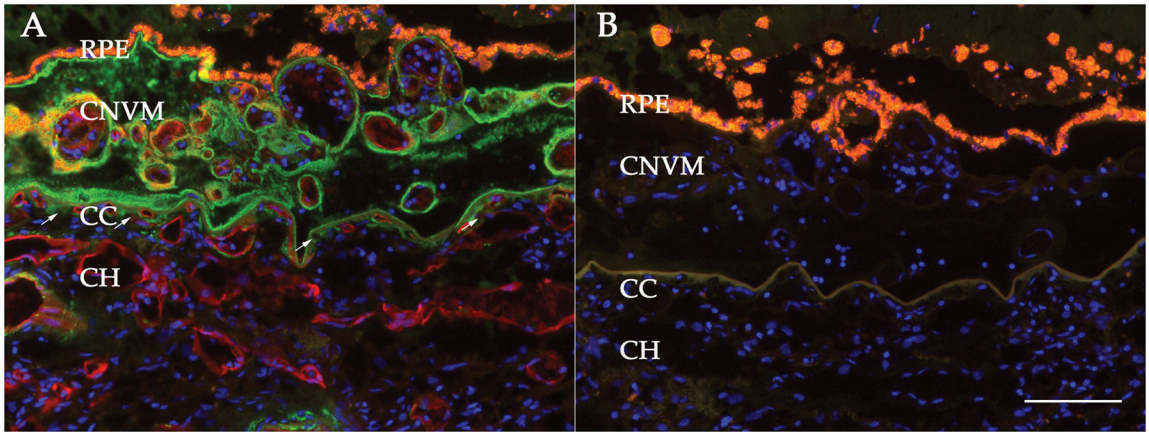

Figure 6. Deposition of the membrane attack complex in an eye with choroidal neovascularization

Section from a 70 year old female donor, showing labeling of the MAC (green) and the vascular marker UEA-I (red). Nuclei are counterstained with DAPI (blue). Note the presence of choriocapillaris ghost vessels (arrows). In some cases, MAC is observed around vessels within the CNVM, consistent with findings of MAC as an activator of angiogenesis-associated genes. Right panel, adjacent section with omission of the primary antibody and lectin. Scale bar = 100 μm.

Table 1

Forty most differentially expressed genes between MAC treated and control RF/6A cells.

Ensembl ID	Symbol	Description	Chromosome	Length	MAC (FPKM)	Control (FPKM)	Log_2 (fold change)	p-value	q-value
ENSMMUT00000002555	ENSMMUG00000001815	Novel pseudogene	chr2	281	5.70	0.00	Inf	0.000050	0.000223
ENSMMUT00000009755	NPPC	C-type natriuretic peptide	chr12	381	3.92	0.00	Inf	0.000050	0.000223
ENSMMUT00000018313	HAS1	hyaluronan synthase 1	chr19	2119	10.90	0.15	6.19	0.000050	0.000223
ENSMMUT00000046604	NR4A1	nuclear receptor subfamily 4, group A, member 1	chr11	2433	208.42	5.40	5.27	0.000050	0.000223
ENSMMUT00000023682	PTGS2	Prostaglandin-endoperoxide synthase 2 (prostaglandin G/H synthase and cyclooxygenase)	chr1	3378	91.08	2.44	5.22	0.000050	0.000223
ENSMMUT00000003274	AREGB	Amphiregulin	chr5	1239	41.34	1.20	5.11	0.000050	0.000223
ENSMMUT00000016263	NR4A2	Nuclear receptor subfamily 4 group A member 2	chr12	3452	57.21	2.17	4.72	0.000050	0.000223
ENSMMUT00000006027	MMP3	matrix metallopeptidase 3 (stromelysin 1, progelatinase)	chr14	1817	9.16	0.37	4.64	0.000050	0.000223
ENSMMUT00000032267	NR4A1	nuclear receptor subfamily 4, group A, member 1	chr11	2616	11.58	0.56	4.37	0.000050	0.000223
ENSMMUT00000023244	MMP9	Matrix metalloproteinase-9; Matrix metalloproteinase-9 preproprotein	chr10	2319	44.88	2.30	4.29	0.000050	0.000223
ENSMMUT00000027899	BMP2	Bone morphogenetic protein 2	chr10	2818	1.53	0.08	4.26	0.000100	0.000428
ENSMMUT00000033070	FGF1	fibroblast growth factor 1 (acidic)	chr6	889	38.26	2.03	4.24	0.000050	0.000223
ENSMMUT00000027604	CEBPE	CCAAT/enhancer binding protein (C/EBP), epsilon	chr7	1551	2.34	0.14	4.08	0.000050	0.000223
ENSMMUT00000012388	STC1	Stanniocalcin-1	chr8	2331	145.40	8.77	4.05	0.000050	0.000223
ENSMMUT00000030710	SEMA7A	Semaphorin-7A isoform 1 preproprotein	chr7	2070	250.88	15.71	4.00	0.000050	0.000223
ENSMMUT00000015976	NR4A3	nuclear receptor subfamily 4, group A, member 3	chr15	3803	8.98	0.59	3.92	0.000050	0.000223
ENSMMUT00000013772	DUSP5	dual specificity phosphatase 5	chr9	2481	179.86	12.35	3.86	0.000050	0.000223
ENSMMUT00000007904	PCDH9	Protocadherin-9 isoform 2	chr17	3612	2.01	0.14	3.82	0.000050	0.000223
ENSMMUT00000013738	SHC4	Src-like proteiny 2 domain-containing-transforming protein C4	chr7	4574	8.39	0.62	3.76	0.000050	0.000223
ENSMMUT00000002085	LAMC2	laminin, gamma 2	chr1	3582	11.48	0.86	3.74	0.000050	0.000223

Ensembl ID	Symbol	Description	Chromosome	Length	MAC (FPKM)	Control (FPKM)	Log_2 (fold change)	p-value	q-value
ENSMMUT00000023885	DCN	decorin	chr11	1936	129.98	673.77	−2.37	0.000050	0.000223
ENSMMUT00000047353	SCMH1	sex comb on midleg homolog 1 (Drosophila)	chr1	3248	0.37	1.99	−2.42	0.000150	0.000623
ENSMMUT00000001585	INHBE	inhibin, beta E	chr11	1613	3.43	19.19	−2.49	0.000050	0.000223
ENSMMUT00000039895	CTAGE5	Cutaneous T-cell lymphoma-associated antigen 5 isoform 2	chr7	2908	1.09	6.11	−2.49	0.000050	0.000223
ENSMMUT00000023887	DCN	decorin	chr11	1835	27.19	153.90	−2.50	0.000050	0.000223
ENSMMUT00000000387	ADAMTS9	ADAM metallopeptidase with thrombospondin type 1 motif, 9	chr2	7315	3.36	20.21	−2.59	0.000050	0.000223
ENSMMUT00000014002	TGFBR2	transforming growth factor, beta receptor II (70/80kDa)	chr2	1704	3.54	21.75	−2.62	0.000050	0.000223
ENSMMUT00000022563	ITGA10	integrin, alpha 10	chr1	5173	1.39	8.52	−2.62	0.000050	0.000223
ENSMMUT00000024656	IFIT1	interferon-induced protein with tetratricopeptide repeats 1	chr9	1772	1.60	10.26	−2.68	0.000050	0.000223
ENSMMUT00000026149	ABCA9	ATP-binding cassette, sub-family A (ABC1), member 9	chr16	5150	0.26	1.66	−2.68	0.000050	0.000223
ENSMMUT00000031010	SP7	Sp7 transcription factor	chr11	3176	0.18	1.20	−2.74	0.000050	0.000223
ENSMMUT00000011159	PLSCR4	phospholipid scramblase 4	chr2	3172	5.94	40.23	−2.76	0.000050	0.000223
ENSMMUT00000001442	HSD11B1	hydroxysteroid (11-beta) dehydrogenase 1	chr1	1343	0.63	4.29	−2.77	0.000050	0.000223
ENSMMUT00000042190	CXCL1	Macaca mulatta chemokine (C-X-C motif) ligand 1 (melanoma growth stimulating activity, alpha) (CXCL1), mRNA.	chr5	1017	53.84	373.25	−2.79	0.000050	0.000223
ENSMMUT00000028195	NRP2	neuropilin 2	chr12	3350	0.56	3.93	−2.81	0.000050	0.000223
ENSMMUT00000039671	ENTPD5	ectonucleoside triphosphate diphosphohydrolase 5	chr7	1964	0.20	1.42	−2.84	0.000250	0.000997
ENSMMUT00000027620	PIK3IP1	phosphoinositide-3-kinase interacting protein 1	chr10	2414	0.25	2.03	−3.00	0.000050	0.000223
ENSMMUT00000027799	IL1B	Macaca mulatta interleukin 1, beta (IL1B), mRNA.	chr13	1480	0.97	8.27	−3.09	0.000050	0.000223
ENSMMUT00000025665	MX1	Macaca mulatta myxovirus (influenza virus) resistance 1, interferon-inducible protein p78 (mouse) (MX1), mRNA.	chr3	786	0.70	6.42	−3.20	0.000050	0.000223
ENSMMUT00000010253	TXNIP	Thioredoxin-interacting protein	chr1	2796	23.71	261.85	−3.47	0.000050	0.000223

Table 2

Most specific GO terms enriched in the top 200 differentially expressed genes

We defined terminal terms as GO terms within the WebGestalt hierarchy having no child terms. The mean $\log_2$(fold change) was calculated after removing genes with infinite fold change (i.e., zero expression within the controls). “Position” refers to the maximum depth in the from the root node (“biological process” at position 0).

Term ID	Term	Position	No. genes in term	No. genes in term from top 200	Bonferroni adjusted p-value	Mean $\log_2$(fold change)
GO:0048514	blood vessel morphogenesis	9	433	24	5.46e-08	2.68
GO:0030335	positive regulation of cell migration	7	226	18	4.82e-08	2.81
GO:0022603	regulation of anatomical structure morphogenesis	5	591	29	8.65e-09	2.57
GO:0048646	anatomical structure formation involved in morphogenesis	5	1594	55	1.95e-12	2.61
GO:0009888	tissue development	4	1449	45	5.83e-08	2.58
GO:0042127	regulation of cell proliferation	4	1177	40	6.21e-08	2.53
GO:0051094	positive regulation of developmental process	4	682	31	1.08e-08	2.76
GO:2000026	regulation of multicellular organismal development	4	1098	38	1.25e-07	2.61
GO:0007154	cell communication	3	4770	93	3.26e-08	2.53
GO:0023052	signaling	1	4646	90	1.54e-07	2.51
GO:0040007	growth	1	796	33	2.49e-08	2.73